Syntheses, crystal structures, dye degradation and luminescence sensing properties of four coordination polymers

Ling Qin[a,b,c], Qing Hu[c], Qi-Ming Zheng[c], Yue Dou[c], Hu Yang[b,*], He-Gen Zheng[a,*]

[a]*State Key Laboratory of Coordination Chemistry, School of Chemistry and Chemical Engineering, Collaborative Innovation Center of Advanced Microstructures, Nanjing University, Nanjing 210023, P. R. China*

[b]*School of the environment, Nanjing University, Nanjing 210023, P. R. China*

[c]*School of Chemistry and Chemical Engineering, Hefei University of Technology, Hefei, 230009, Anhui, P. R. China*

Materials and methods

All reagents were of analytical grade and used without further purification. C, H and N elemental analyses were carried out with a Perkin Elmer 240C elemental analyzer. Powder X-ray diffraction (PXRD) measurements were performed on a Bruker D8 Advance X-ray diffractometer using Cu-Kα radiation (1.5418 Å), and the X-ray tube was operated at 40 kV and 40 mA. Liquid UV-Vis measurements were conducted on a TU-1900 UV-vis spectrometer. IR absorption spectra of the complexes were recorded in the range 400-4000 cm^{-1} on an Agilent Technologies Carry 630 FTIR spectrometer with KBr pellets (5mg of sample in 500 mg of KBr). Luminescent measurements were conducted on a Perkinelmer LS55. The as-synthesized samples were characterized by thermogravimetric analysis (TGA) on a Perkin Elmer thermogravimetric analyzer Pyris 1 TGA up to 973 K using a heating rate of 10 K

min^{-1} under N_2 atmosphere. Solid-state UV-vis diffuse reflectance spectra were obtained at room temperature using Shimadzu UV-3600 double monochromator spectrophotometer, and $BaSO_4$ was used as a 100% reflectance standard for all materials.

X-ray crystallography

Crystallographic data of **1-4** were collected on a Bruker Apex Smart CCD diffractometer with graphite-monochromated Mo-K_α radiation (λ = 0.71073 Å) at 293 K using the ω-scan technique. The intensity data were integrated by using the SAINT program. An empirical absorption correction was applied using the SADABS program.[1] The structures were solved by direct methods and refined anisotropically using full-matrix least-squares procedures based on F^2 values with the SHELXTL-97 package of crystallographic software.[2] The hydrogen atoms were generated geometrically. The selected bond lengths and angles are given in Table S1. The CCDC reference number is 1936810-1936813 for **1-4**. The data can be obtained free of charge via <http,//www.ccdc.cam.ac.uk/conts/retrieving.html>, or from the Cambridge Crystallographic Data Centre, 12 Union Road, Cambridge CB2 1EZ, UK, fax,(+44) 1223-336-033, or e-mail, deposit@ccdc.cam.ac.uk.

---

1 Bruker. APEX2, SAINT and SADABS, Bruker AXS Inc., Madison, WI (2009).

2 (a) G. M. Sheldrick, *Acta Cryst.*, 2008, **64**, 112; (b) G. M. Sheldrick. *Acta Cryst.*, 2015, **71**, 3.

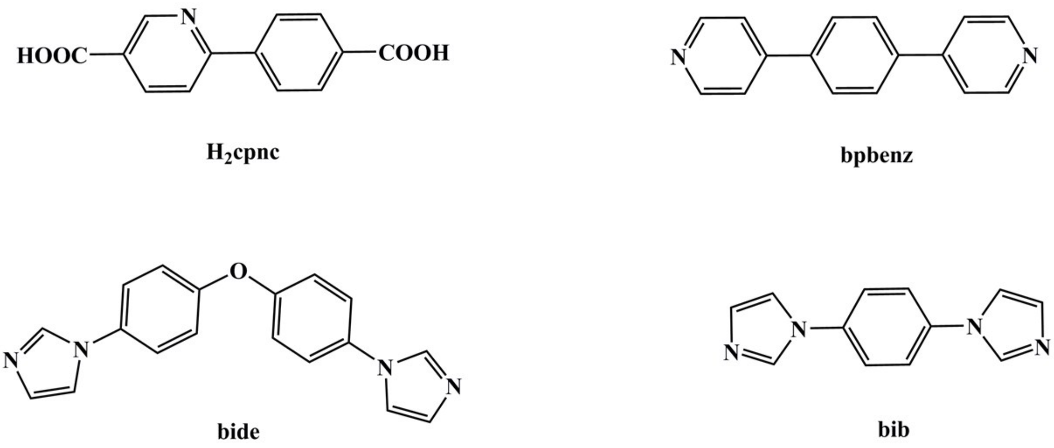

Scheme S1. Mixed ligands used in this article.

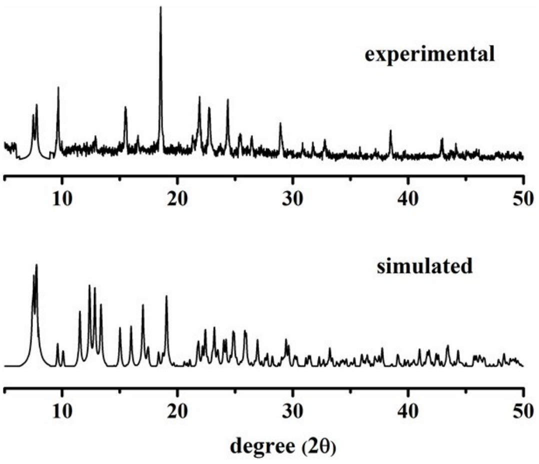

Figure S1. The powder X-ray diffraction patterns (PXRD) of **1**.

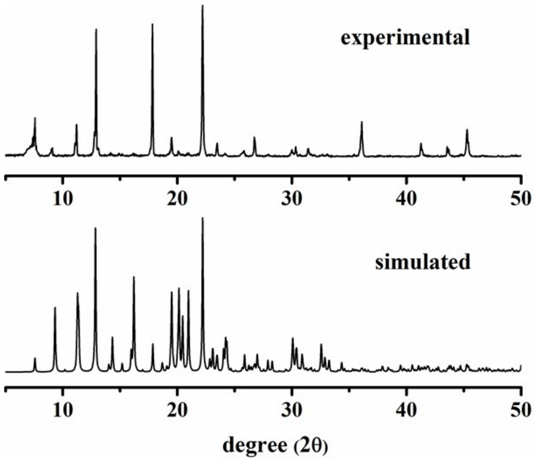

Figure S2. The powder X-ray diffraction patterns (PXRD) of **2**.

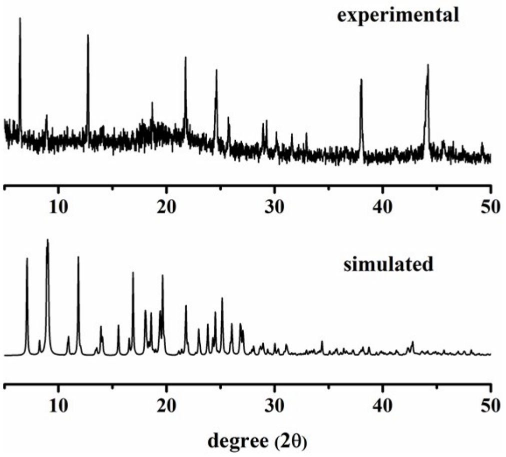

Figure S3. The powder X-ray diffraction patterns (PXRD) of **3**.

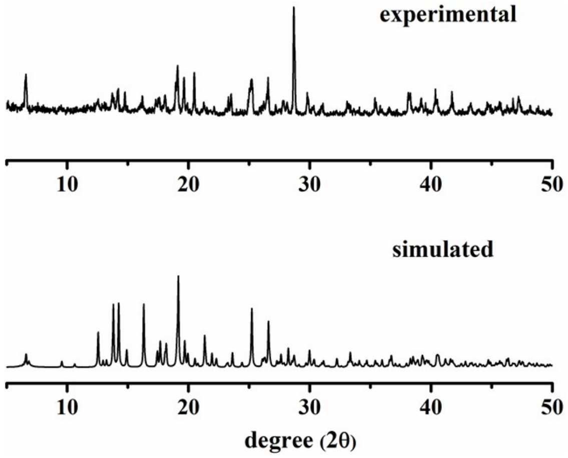

Figure S4. The powder X-ray diffraction patterns (PXRD) of **4**.

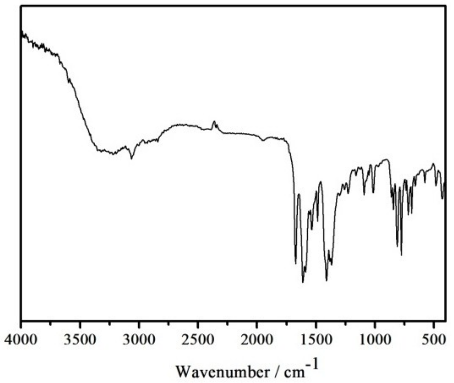

Figure S5. The infrared spectra (IR) of **1**.

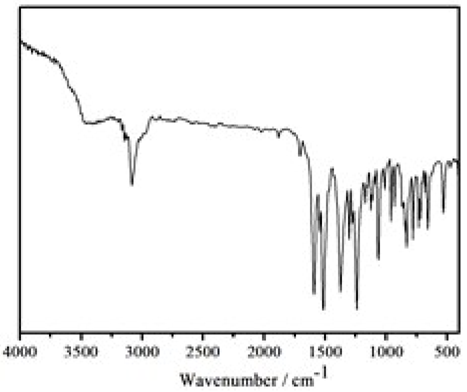

Figure S6. The infrared spectra (IR) of **2**.

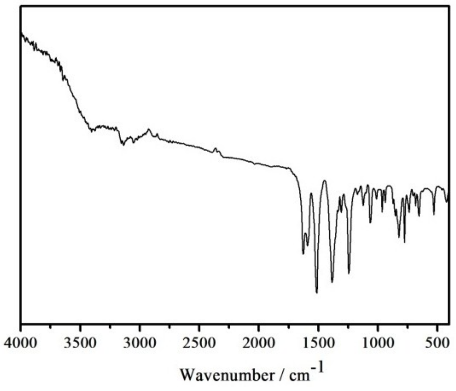

Figure S7. The infrared spectra (IR) of **3**.

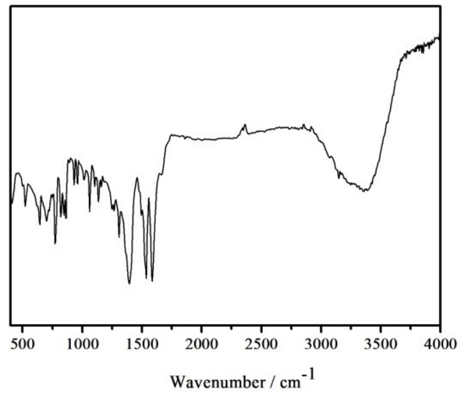

Figure S8. The infrared spectra (IR) of **4**.

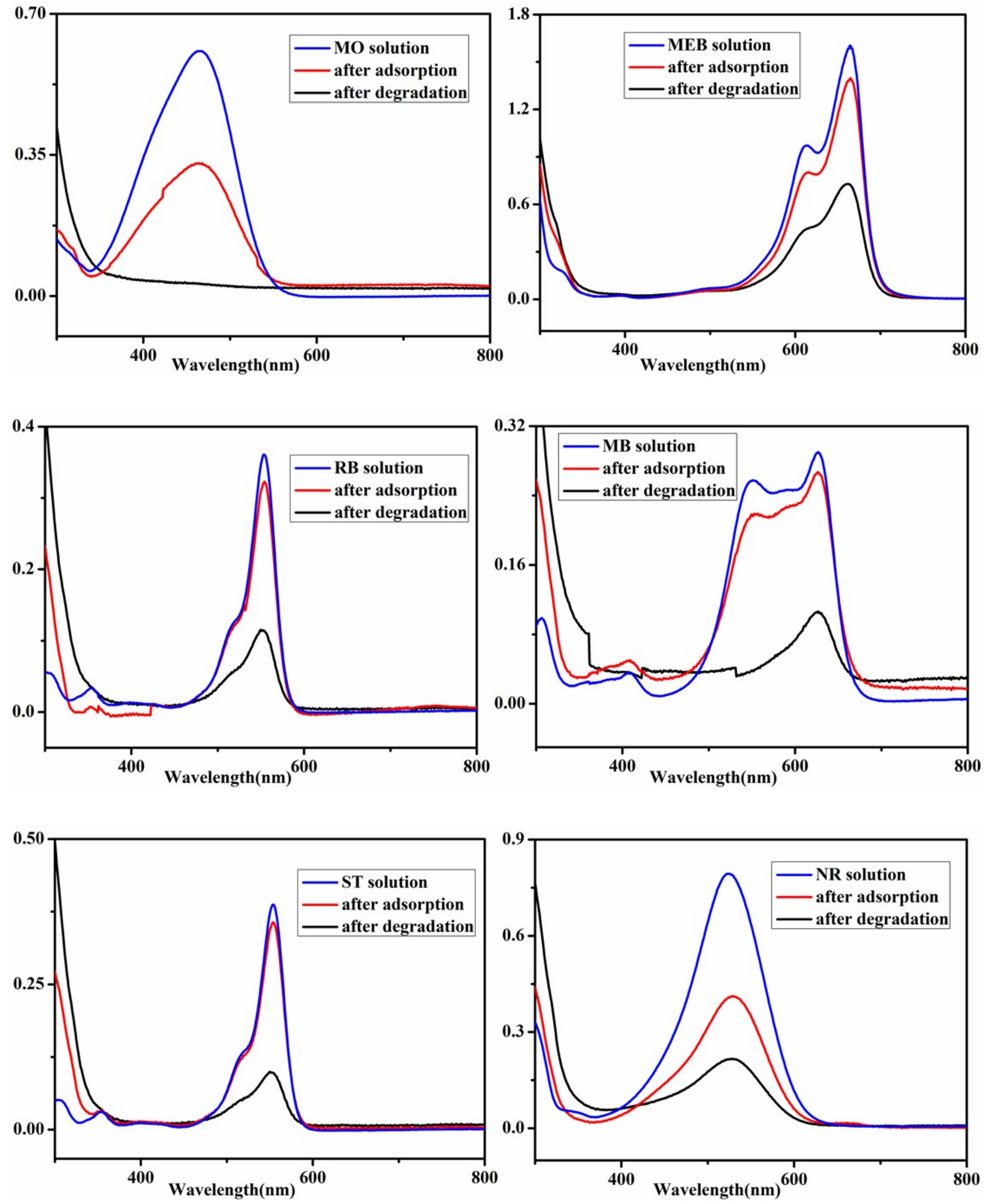

Figure S9. The UV-vis absorption spectra of the dye solutions during the adsorption and degradation reaction in the presence of compound **1**.

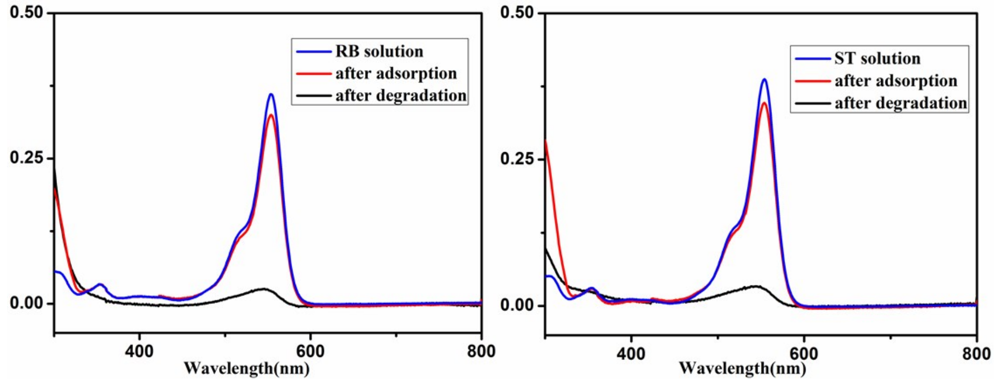

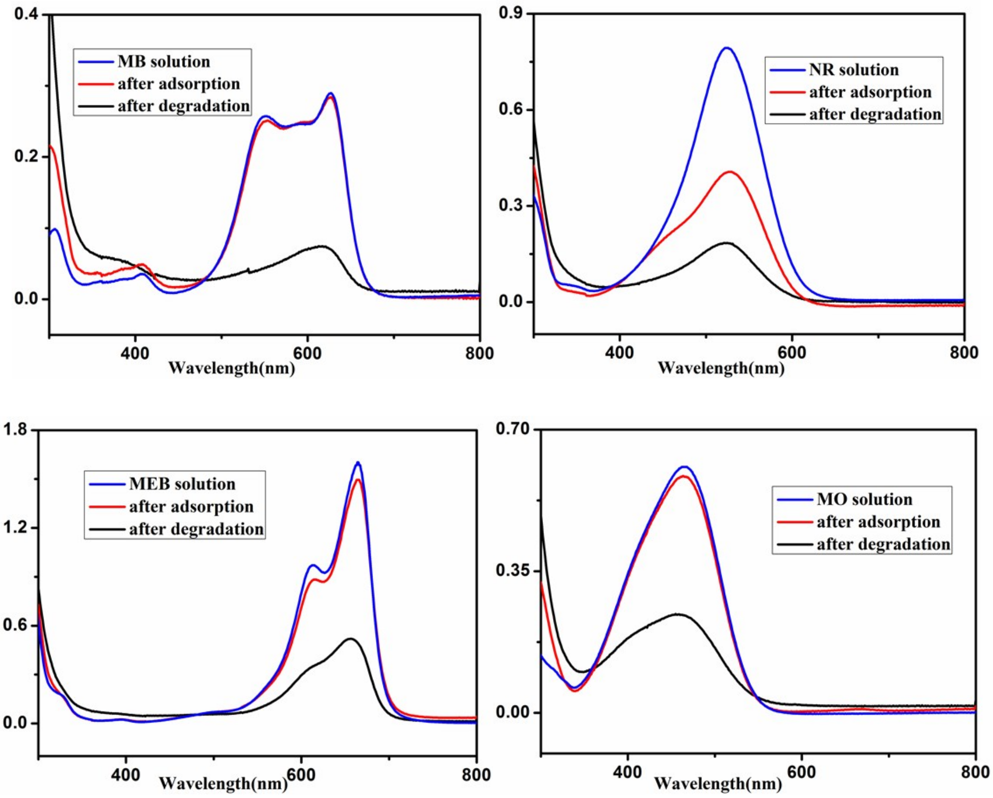

Figure S10. The UV-vis absorption spectra of the dye solutions during the adsorption and degradation reaction in the presence of compound **2**.

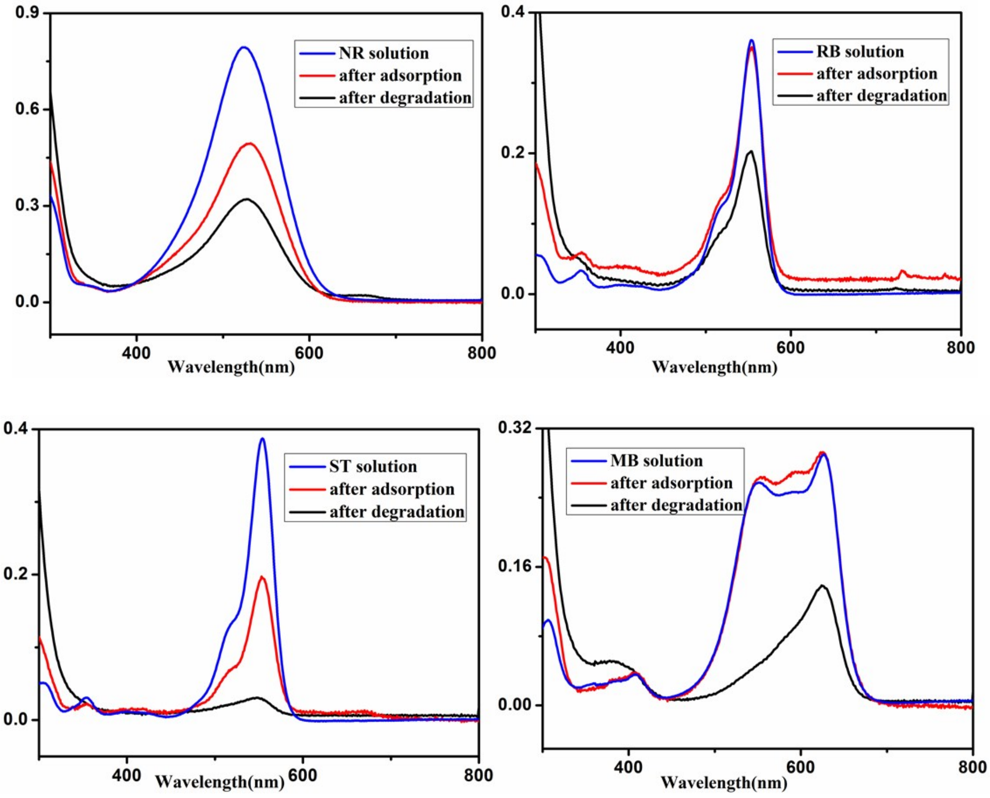

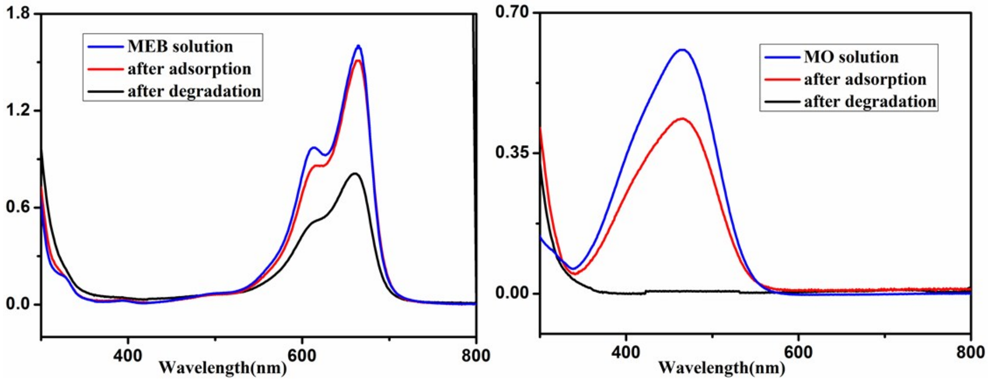

Figure S11. The UV-vis absorption spectra of the dye solutions during the adsorption and degradation reaction in the presence of compound **3**.

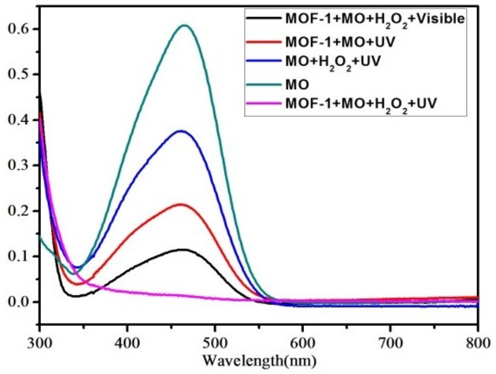

Figure S12. The UV-vis absorption spectra of the MO dye solution for compound **1** during the degradation reaction in four groups of experiments.

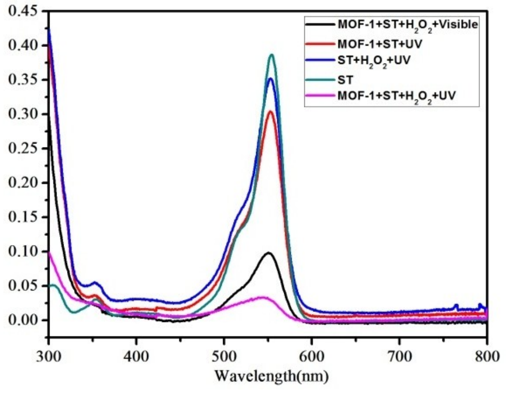

Figure S13. The UV-vis absorption spectra of the ST dye solution for compound **1** during the degradation reaction in four groups of experiments.

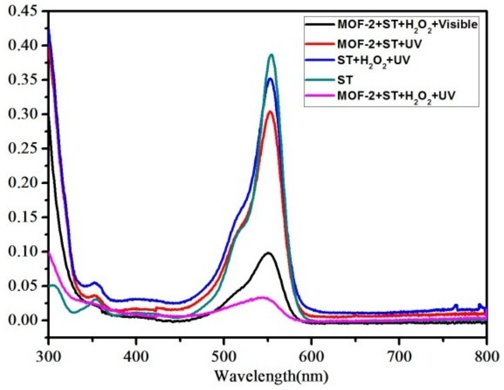

Figure S14. The UV-vis absorption spectra of the ST dye solution for compound **2** during the degradation reaction in four groups of experiments.

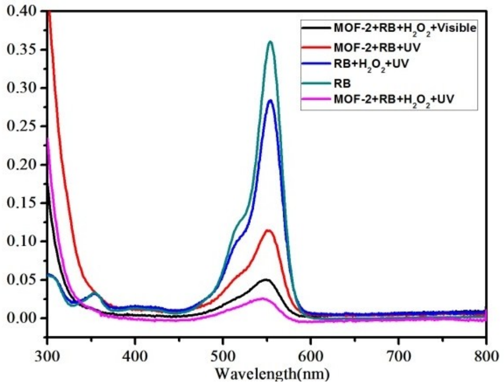

Figure S15. The UV-vis absorption spectra of the RB dye solution for compound **2** during the degradation reaction in four groups of experiments.

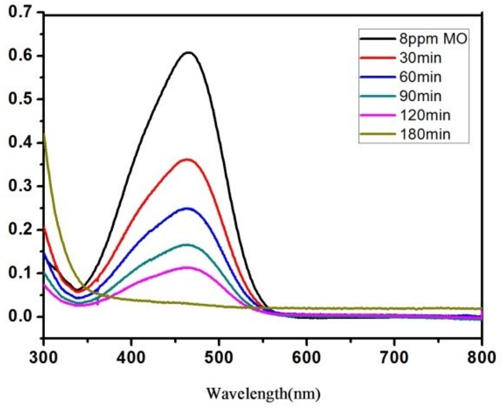

Figure S16. Time dependent UV-vis spectra of 8 mL of 8 ppm MO aqueous solution in the presence of 0.5mL H_2O_2 (30%). The solution contains 5 mg of **1**.

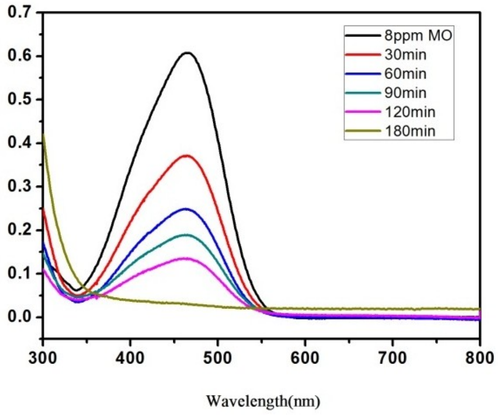

Figure S17. Time dependent UV-vis spectra of 8 mL of 8 ppm MO aqueous solution in the presence of 0.5mL H_2O_2 (30%). The solution contains 10 mg of **1**.

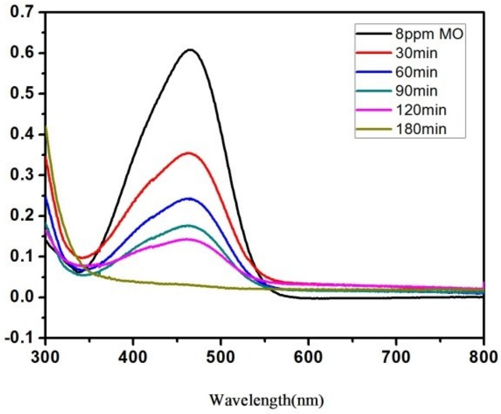

Figure S18. Time dependent UV-vis spectra of 8 mL of 8 ppm MO aqueous solution in the presence of 0.5mL H_2O_2 (30%). The solution contains 15 mg of **1**.

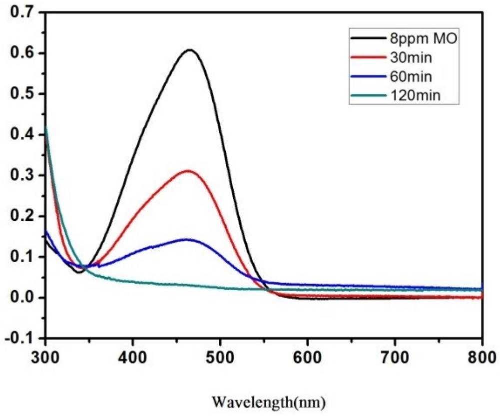

Figure S19. Time dependent UV-vis spectra of 8 mL of 8 ppm MO aqueous solution in the presence of 0.5mL H_2O_2 (30%). The solution contains 20 mg of **1**.

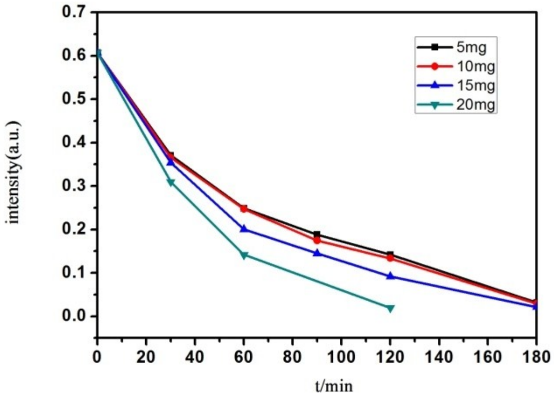

Figure S20. Change of absorption of the solution of MO in the presence of 0.5 mL H_2O_2 with different catalyst **1** concentrations (5mg, 10mg, 15mg, and 20mg) under exposure of UV light at room temperature.

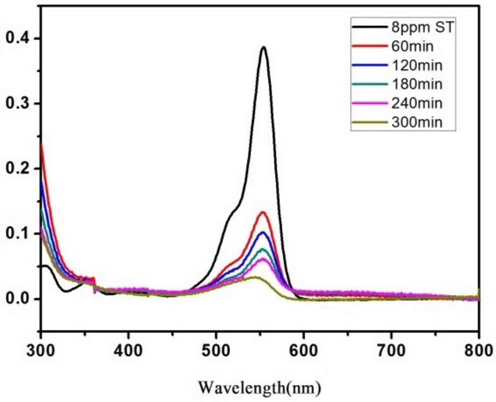

Figure S21. Time dependent UV-vis spectra of 8 mL of 8 ppm ST aqueous solution in the presence of 0.5mL H_2O_2 (30%). The solution contains 5 mg of **2**.

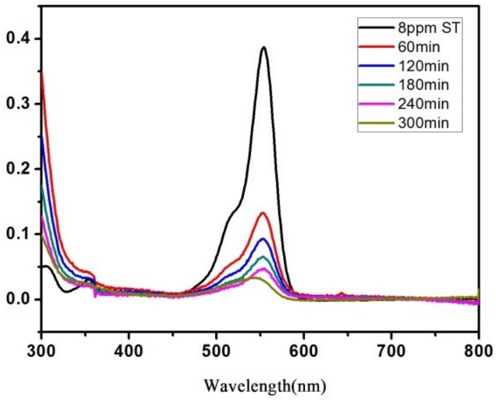

Figure S22. Time dependent UV-vis spectra of 8 mL of 8 ppm ST aqueous solution in the presence of 0.5mL H_2O_2 (30%). The solution contains 10 mg of **2**.

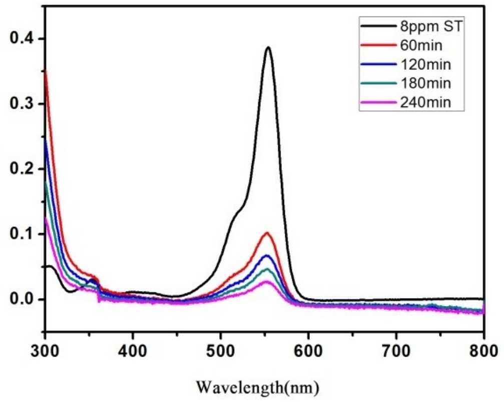

Figure S23. Time dependent UV-vis spectra of 8 mL of 8 ppm ST aqueous solution in the presence of 0.5mL H_2O_2 (30%). The solution contains 15 mg of **2**.

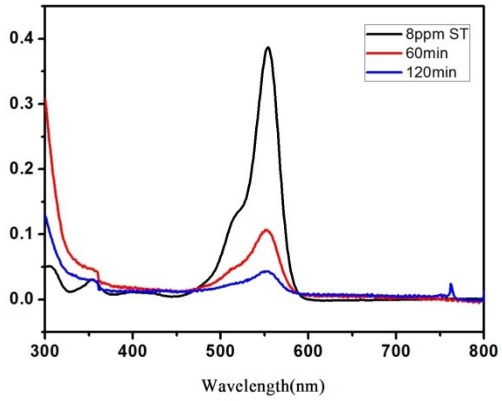

Figure S24. Time dependent UV-vis spectra of 8 mL of 8 ppm ST aqueous solution in the presence of 0.5mL H_2O_2 (30%). The solution contains 20 mg of **2**.

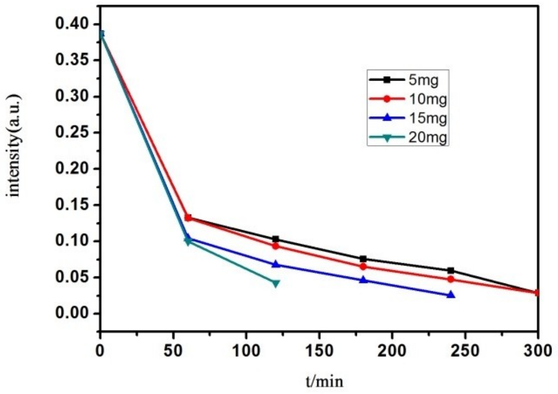

Figure S25. Change of absorption of the solution of ST in the presence of 0.5 mL H_2O_2 with different catalyst **2** concentrations (5mg, 10mg, 15mg, and 20mg) under exposure of UV light at room temperature.

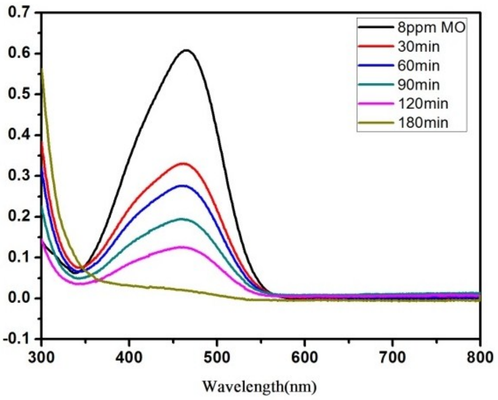

Figure S26. Time dependent UV-vis spectra of 8 mL of 8 ppm MO aqueous solution in the presence of 10 mg of **1**. The solution contains 0.25mL H_2O_2 (30%).

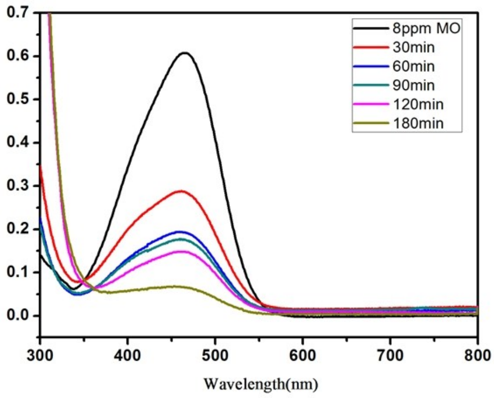

Figure S27. Time dependent UV-vis spectra of 8 mL of 8 ppm MO aqueous solution in the presence of 10 mg of **1**. The solution contains 0.5mL H_2O_2 (30%).

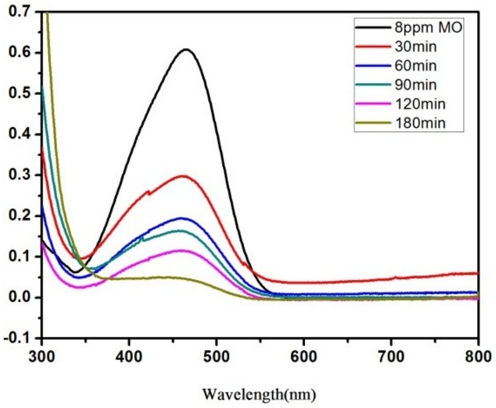

Figure S28. Time dependent UV-vis spectra of 8 mL of 8 ppm MO aqueous solution in the presence of 10 mg of **1**. The solution contains 0.75mL H_2O_2 (30%).

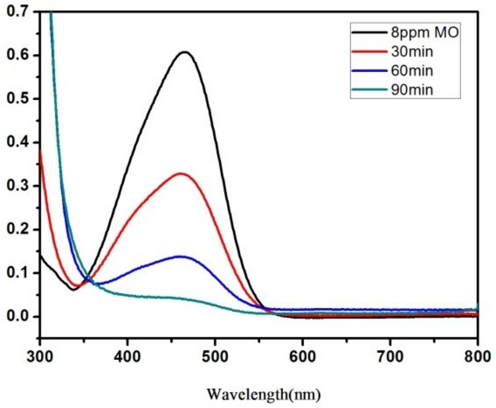

Figure S29. Time dependent UV-vis spectra of 8 mL of 8 ppm MO aqueous solution in the presence of 10 mg of **1**. The solution contains 1.0mL H_2O_2 (30%).

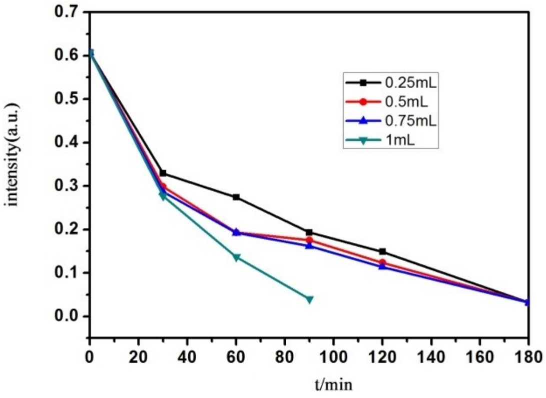

Figure S30. Change of absorption of the solution of MO in the presence of 10 mg of **1** with different H_2O_2 concentrations under exposure of UV light at room temperature.

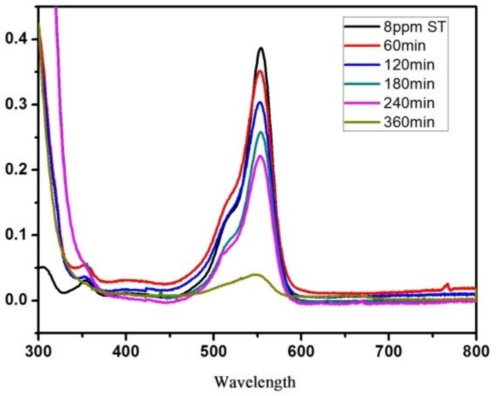

Figure S31. Time dependent UV-vis spectra of 8 mL of 8 ppm ST aqueous solution in the presence of 10 mg of **2**. The solution contains 0.25 mL H_2O_2 (30%).

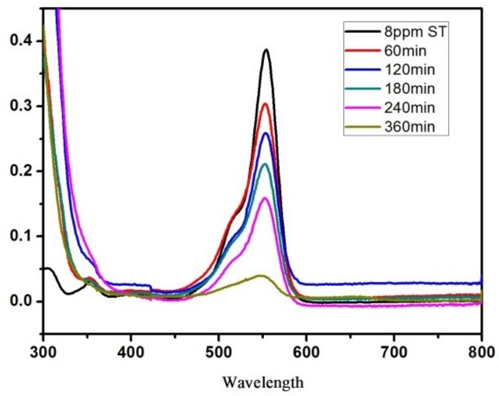

Figure S32. Time dependent UV-vis spectra of 8 mL of 8 ppm ST aqueous solution in the presence of 10 mg of **2**. The solution contains 0.5 mL H_2O_2 (30%).

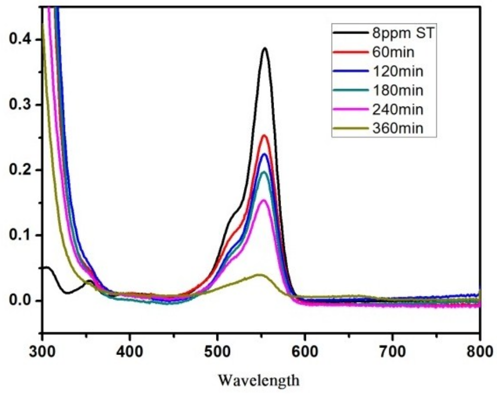

Figure S33. Time dependent UV-vis spectra of 8 mL of 8 ppm ST aqueous solution in the presence of 10 mg of **2**. The solution contains 0.75 mL H_2O_2 (30%).

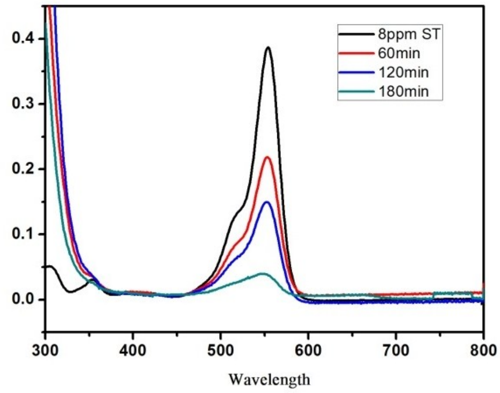

Figure S34. Time dependent UV-vis spectra of 8 mL of 8 ppm ST aqueous solution in the presence of 10 mg of **2**. The solution contains 1.0 mL H_2O_2 (30%).

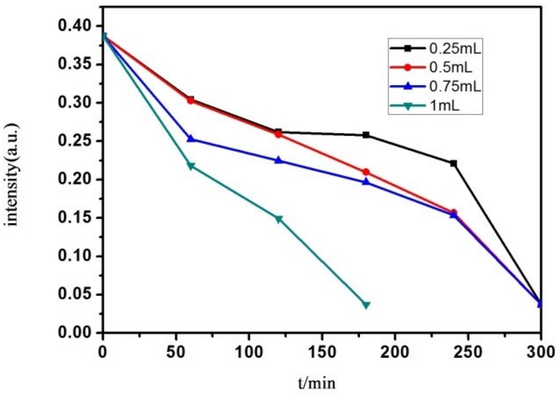

Figure S35. Change of absorption of the solution of MO in the presence of 10 mg of **1** with different H_2O_2 concentrations under exposure of UV light at room temperature.

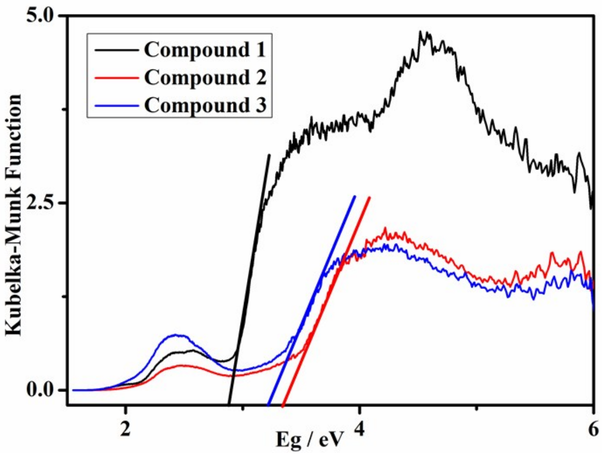

Figure S36. Plot of Kubelka-Munk as a function of energy of the **1**, **2**, and **3** at room temperature.

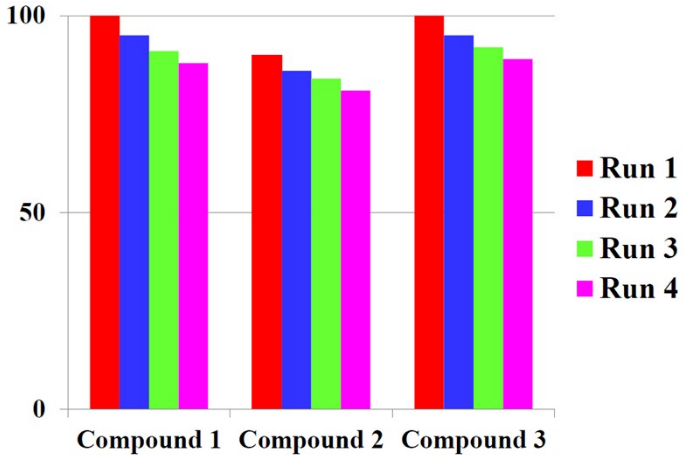

Figure S37. The reusabilities of these catalysts were evaluated by 8.0 ppm dyes degradation (MO for compounds **1** and **3** or ST for compound **2**) in the presence of H_2O_2.

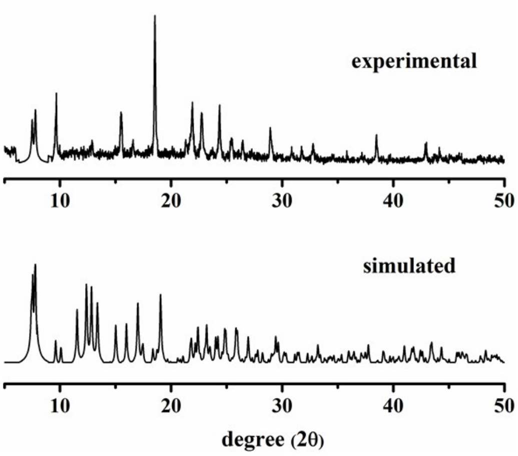

Figure S38. The PXRD for degradation of catalyst **1** for MO dyes.

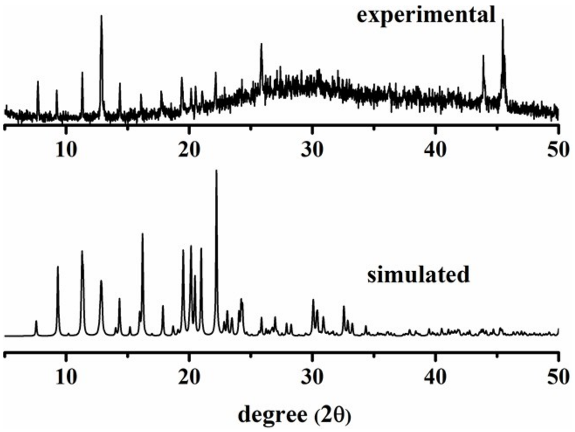

Figure S39. The PXRD for degradation of catalyst **2** for ST dyes.

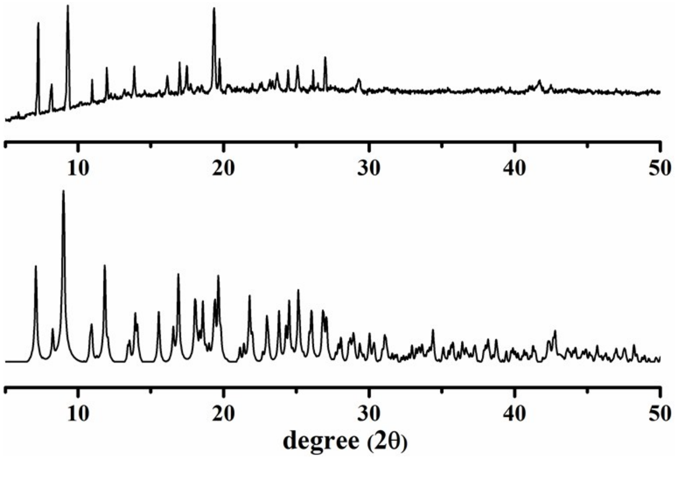

Figure S40. The PXRD for degradation of catalyst **3** for MO dyes.

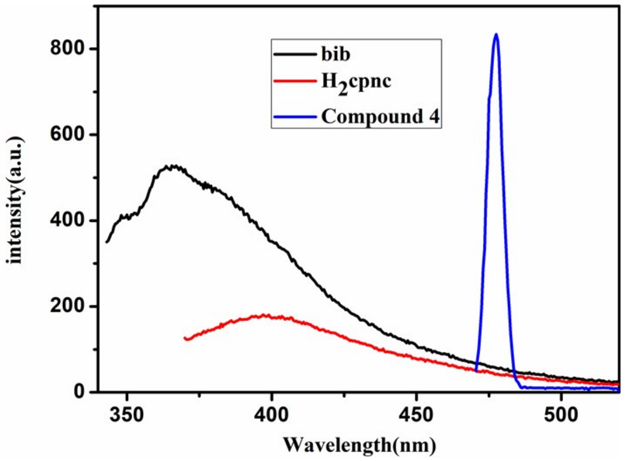

Figure S41. Solid-state photoluminescent spectra of compound **4**, H_2cpnc and bib ligand at room temperature**.**

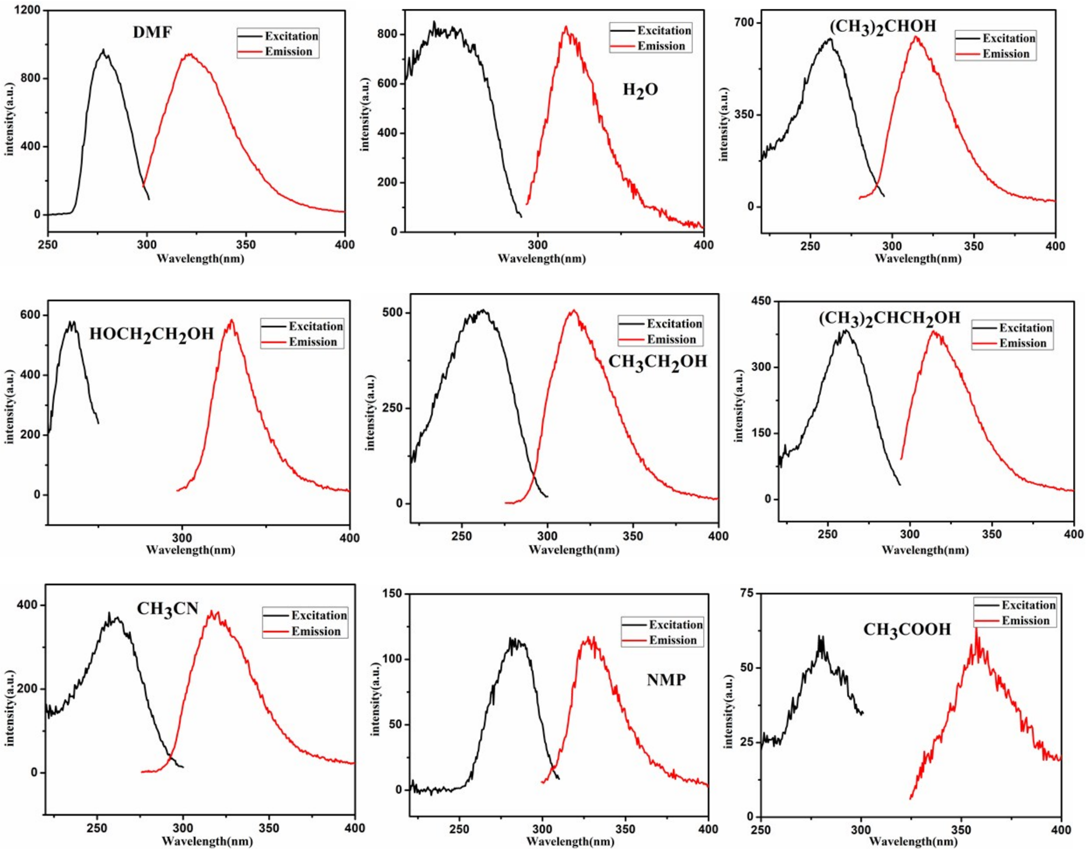

Figure S42. Luminescence spectra of **4** in the presence of different organic solvents with a concentration of 8 mg/10mL.

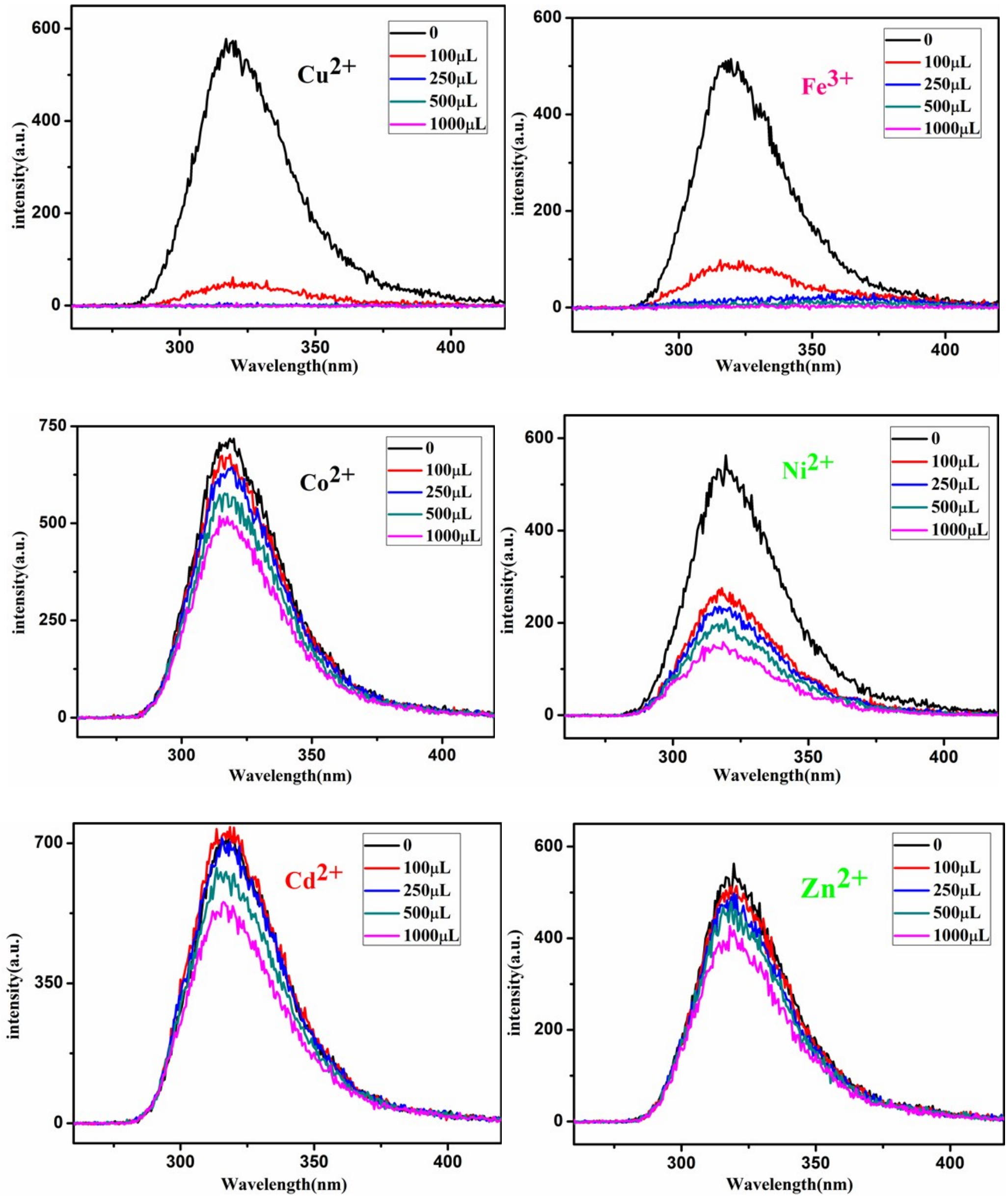

Figure S43. The luminescence responses of **4** dispersed in aqueous solution for metal ion: Concentration-dependent luminescence quenching of **4** after adding different concentrations of $M(NO_3)_2$ ion.

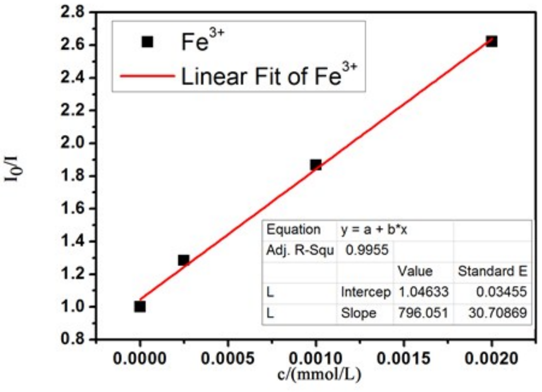

Equation	y = a + b*x		
Adj. R-Squ	0.9955		
		Value	Standard E
L	Intercep	1.04633	0.03455
L	Slope	796.051	30.70869

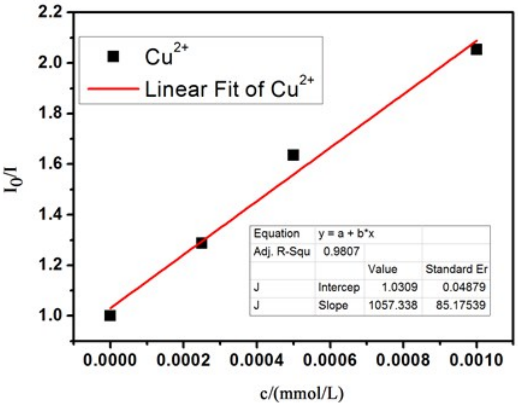

Equation	y = a + b*x		
Adj. R-Squ	0.9807		
		Value	Standard Er
J	Intercep	1.0309	0.04879
J	Slope	1057.338	85.17539

Figure S44. (left) Linear relationship of luminescence quenching for titration of **4**-H_2O with low concentration Cu^{2+}. (right) Linear relationship of luminescence quenching for titration of 1-H_2O with low concentration Fe^{3+}.

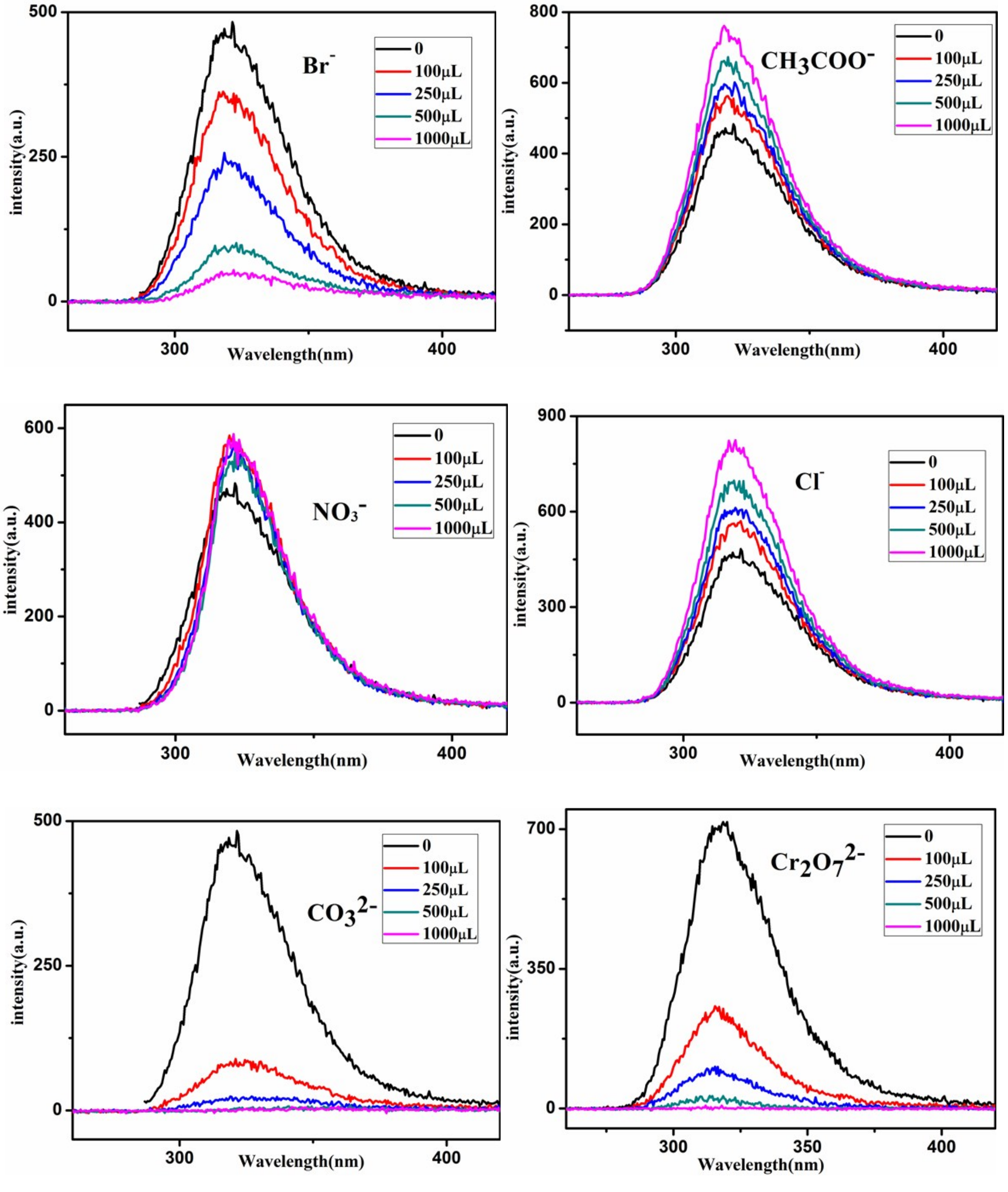

Figure S45. The luminescence responses of **4** dispersed in aqueous solution for KX ion: Concentration-dependent luminescence quenching of **4** after adding different concentrations of KX ion (X= Cl^-, Br^-, CH_3COO^-, NO_3^-, CO_3^{2-}, and $Cr_2O_7^{2-}$).

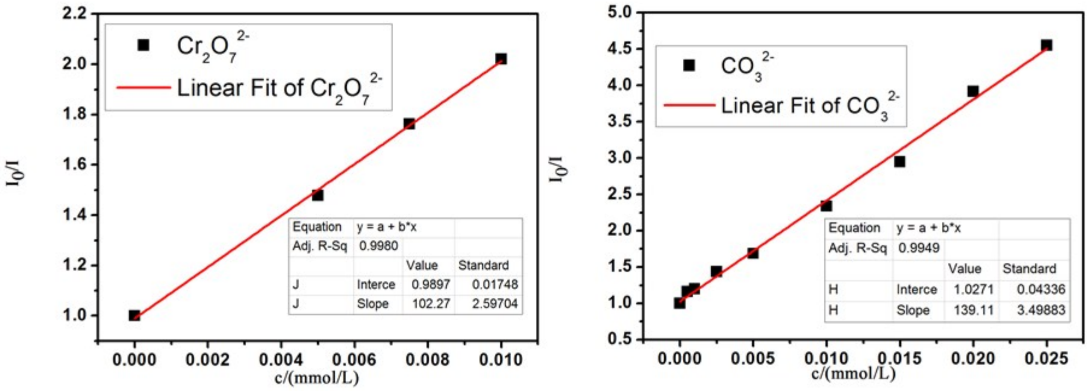

Figure S46. (left) Linear relationship of luminescence quenching for titration of **4**-H_2O with low concentration $Cr_2O_7^{2-}$. (right) Linear relationship of luminescence quenching for titration of 1-H_2O with low concentration CO_3^{2-}.

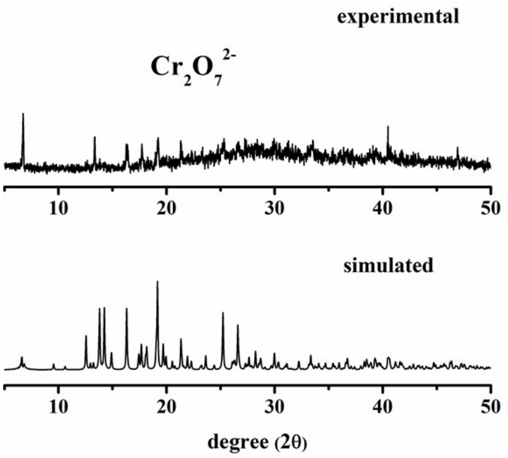

Figure S47. Stability of **4** after the titration experiments for $Cr_2O_7^{2-}$ ion.

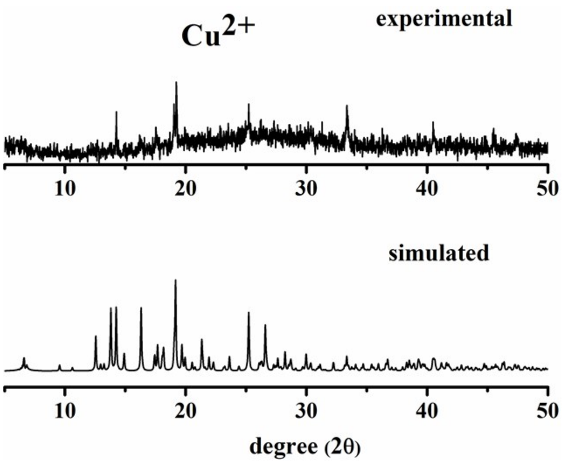

Figure S48. Stability of **4** after the titration experiments for Cu^{2+} ion.

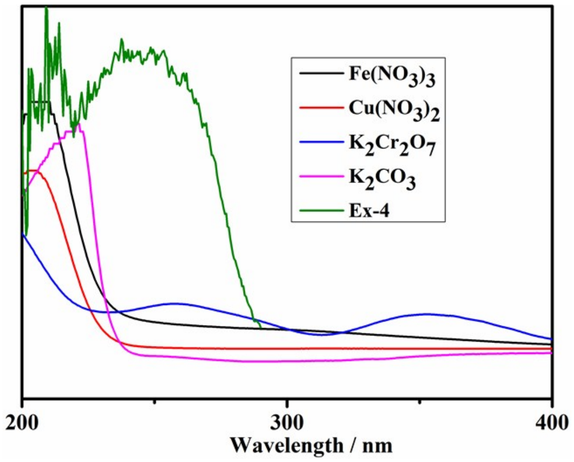

Figure S49. The UV-Vis absorption of $K_2Cr_2O_7$, K_2CO_3, $Fe(NO_3)_3$, $Cu(NO_3)_2$ and the photoluminescent excitation spectra for compound **4**.

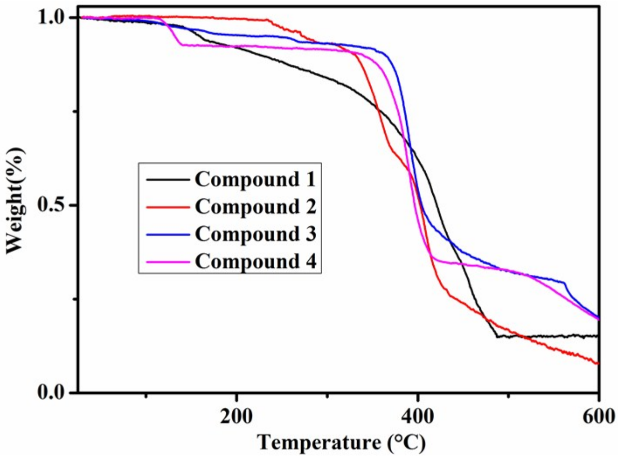

Figure S50. TGA curves for compounds **1**-**4**.

Table S1. Selected Bond Lengths (Å) and Angles (deg) for Compounds **1**-**4**.

Compound **1**

Co1-O1	2.0167(14)	Co1-N1	2.1369(17)
Co1-N2a	2.1437(17)	Co1-O3b	2.1597(14)
Co1-O4b	2.2046(15)	Co1-O2c	2.0388(14)
O1-Co1-N1	87.16(6)	O1-Co1-N2a	91.87(6)
O1-Co1-O3b	153.19(6)	O1-Co1-O4b	92.82(5)
O1-Co1-C13b	122.91(6)	O1-Co1-O2c	117.66(6)
N1-Co1-N2a	178.36(6)	O3b-Co1-N1	92.47(6)
O4b-Co1-N1	88.17(6)	N1-Co1-C13b	90.32(6)
O2c-Co1-N1	87.26(6)	O3b-Co1-N2a	87.81(6)
O4b-Co1-N2a	90.56(6)	N2a-Co1-C13b	89.10(6)
O2c-Co1-N2a	94.36(6)	O3b-Co1-O4b	60.38(5)
O3b-Co1-C13b	30.29(6)	O2c-Co1-O3b	89.07(6)
O4b-Co1-C13b	30.10(6)	O2c-Co1-O4b	148.87(6)
O2c-Co1-C13b	119.15(6)		

Symmetry codes: a=1+x, y,1+z; b= 2-x,1/2+y,3/2-z; c= 1-x,1-y,2-z.

Compound **2**

Co1-O2	2.1294(17)	Co1-N1	2.144(2)
Co1-N4a	2.163(2)	Co1-N4b	2.163(2)
Co1-O2c	2.1294(17)	Co1-N1c	2.144(2)
O2-Co1-N1	91.95(7)	O2-Co1-N4a	86.01(7)
O2-Co1-N4b	94.00(7)	O2-Co1-O2c	180.00
O2-Co1-N1c	88.06(7)	N1-Co1-N4a	92.09(9)
N1-Co1-N4b	87.91(9)	O2c-Co1-N1	88.06(7)
N1-Co1-N1c	180.00	N4a-Co1-N4b	180.00
O2c-Co1-N4a	94.00(7)	N1c-Co1-N4a	87.91(9)
O2c-Co1-N4b	86.01(7)	N1c-Co1-N4b	92.09(9)

O2c-Co1-N1c	91.95(7)

Symmetry codes: a= x,1+y, -1+z; b= 2-x,1-y,1-z; c= 2-x,2-y, -z.

Compound **3**

Co1-O1	2.121(2)	Co1-O1W	2.1558(16)
Co1-N2	2.104(3)	Co1-O2a	2.092(2)
Co1-O3b	2.182(2)	Co1-N5c	2.092(3)
O1-Co1-O1W	95.24(7)	O1-Co1-N2	86.65(9)
O1-Co1-O2a	100.17(9)	O1-Co1-O3b	175.86(9)
O1-Co1-N5c	85.68(9)	O1W-Co1-N2	175.67(8)
O1W-Co1-O2a	88.08(7)	O1W-Co1-O3b	88.38(7)
O1W-Co1-N5c	87.94(9)	O2a-Co1-N2	87.74(10)
O3b-Co1-N2	89.87(9)	N2-Co1-N5c	96.11(10)
O2a-Co1-O3b	81.92(9)	O2a-Co1-N5c	173.21(10)
O3b-Co1-N5c	92.47(9)		

Symmetry codes: a=1-x, y, 1/2-z; b=-1/2+x,1/2-y, -1/2+z; c=1/2+x,1/2-y,1/2+z.

Compound 4

Cd1-O1	2.349(3)	Cd1-O1W	2.360(3)
Cd1-O2	2.748(3)	Cd1-O2W	2.288(3)
Cd1-O3	2.257(2)	Cd1-O4	2.572(3)
Cd1-N2	2.286(3)	O1-Cd1-O1W	76.69(9)
O1-Cd1-O2	50.66(9)	O1-Cd1-O2W	111.02(10)
O1-Cd1-O3	129.34(10)	O1-Cd1-O4	151.95(10)
O1-Cd1-N2	80.47(10)	O1W-Cd1-O2	97.01(9)
O1W-Cd1-O2W	79.08(10)	O1W-Cd1-O3	83.97(9)
O1W-Cd1-O4	127.92(9)	O1W-Cd1-N2	143.26(10)
O2-Cd1-O2W	161.45(9)	O2-Cd1-O3	86.90(9)
O2-Cd1-O4	107.11(9)	O2-Cd1-N2	90.17(11)
O2W-Cd1-O3	110.48(10)	O2W-Cd1-O4	89.14(10)
O2W-Cd1-N2	82.81(12)	O3-Cd1-O4	53.09(9)

O3-Cd1-N2	132.53(10)	O4-Cd1-N2	83.10(9)